Eur. Phys. J. B **30**, 181–187 (2002)
DOI: 10.1140/epjb/e2002-00373-8

THE EUROPEAN PHYSICAL JOURNAL B

Two-step flux penetration in classic antiferromagnetic superconductor

T. Krzysztoń[a] and K. Rogacki

Institute of Low Temperature and Structure Research, Polish Academy of Sciences, 50-950 Wrocław, PO Box 1410, Poland

Received 16 August 2002 / Received in final form 22 October 2002
Published online 29 November 2002

Abstract. The influence of antiferromagnetic order on the mixed state of a superconductor may result in creation of spin-flop domains along vortices. This may happen when an external magnetic field is strong enough to flip over magnetic moments in the vortex core from their ground state configuration. The formation of domain structure causes modification of the surface energy barrier, and creation of the new state in which magnetic flux density is independent of the applied field. The modified surface energy barrier has been calculated for parameters of the antiferromagnetic superconductor $DyMo_6S_8$. The prediction of two-step flux penetration process has been verified by precise magnetization measurements performed on the single crystal of $DyMo_6S_8$ at milikelvin temperatures. A characteristic plateau on the virgin curve $B(H_0)$ has been found and attributed to the modified surface energy barrier. The end of the plateau determines the critical field, which we call the second critical field for flux penetration.

PACS. 74.60.-w Type-II superconductivity – 74.25.Ha Magnetic properties

Introduction

The discoveries of ternary Rare Earth (RE) Chevrel phases $REMo_6S_8$ [1] and $RERh_4B_4$ compounds with regular distribution of localized magnetic moments of RE atoms have proved conclusively the coexistence of various types of magnetism with superconductivity. Intensive experimental and theoretical works have shown that $4f$ electrons of RE atoms responsible for magnetism and $4d$ electrons of molybdenum chalcogenide or rhodium boride clusters responsible for superconductivity are spatially separated and therefore their interaction is weak. It seems that in many of these systems superconductivity coexists rather easily with antiferromagnetic order, where usually the Néel temperature T_N is lower than the critical temperature for superconductivity T_c. On the other hand, ferromagnetism and superconductivity cannot coexist in bulk samples with realistic parameters. Quite often the ferromagnetic order is transformed into a spiral or domain-like structure, depending on the type and strength of magnetic anisotropy in the system [2,3]. For almost two decades the problem of the interaction between magnetism and superconductivity has been overshadowed by high temperature superconductivity found in copper oxides. However, the recent discovery of the presence of magnetic order in Ru-based superconductors [4–6] has triggered a new series of experiments and inspired a return to the so-called coexistence phenomenon [7]. Most recently, the interplay between magnetism and superconductivity was studied in d-electron UGe_2 [8] and $ZrZn_2$ [9], where itinerant ferromagnetism may coexist with superconductivity, and in heavy fermion UPd_2Al_3 [10], where magnetic excitons are present in superconducting phase.

Among classical magnetic superconductors, the Chevrel phases have been studied most intensively. These compounds are mainly polycrystalline materials. However, some specific features can be measured only on single crystals. One such effect is a two-step flux penetration process, predicted in references [11,12] and later observed in an antiferromagnetic superconductor (bct) $ErRh_4B_4$ [13] and recently in $DyMo_6S_8$ [14]. This anomaly was explained as a result of the magnetic transition taking place in the vortex core. This transition seems to create a new type of vortices with the unique magnetic structure as shown in Figure 1. In the present paper the two-step flux penetration process is calculated and measured for a single crystal of $DyMo_6S_8$. The $DyMo_6S_8$ compound with $T_c = 1.6$ K exhibits transition from the paramagnetic to the antiferromagnetic state at $T_N = 0.4$ K. Its crystal structure can be described as interconnected Mo_6S_8 units and Dy ions. One such unit is a slightly deformed cube where S atoms sit at the corners and Mo atoms are situated at the cube-faces. The Mo_6S_8 units are arranged in a simple rhombohedral lattice and Dy ions are located in the center of the unit cell. The magnetic moments of Dy ions form a simple structure consisting of (100) planes with moments of 8.7 μ_B alternately parallel and antiparallel to the [111] rhombohedral axis.

[a] e-mail: krzyszto@int.pan.wroc.pl

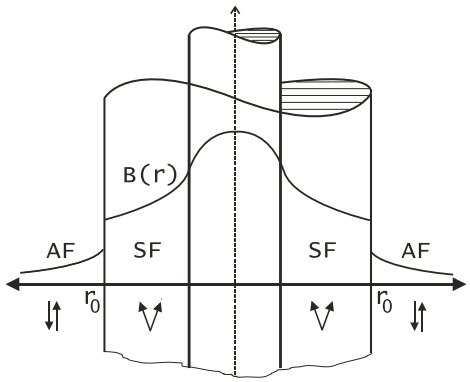

Fig. 1. The magnetic structure of the isolated vortex and the distribution of the magnetic induction around the vortex core in the spin-flop SF and antiferromagnetic AF phases [11].

Neutron experiments performed on $DyMo_6S_8$ in an applied magnetic field at $T = 0.2$ K have revealed in the intensity spectrum a number of peaks characteristic for ferromagnetic order [15]. These peaks begin to develop at $H_0 = 200$ Oe, much below the superconducting upper critical field H_{c2}. Thus, in $DyMo_6S_8$ a kind of ferromagnetic order coexists with superconductivity in the same manner as antiferromagnetism. For a field applied parallel to the [111] direction (magnetic easy-axis direction), the ferromagnetic order is a spin-flop type [16]. This feature is easy to understand. Consider the well known phase diagram of a two-sublattice antiferromagnet. An infinitesimal magnetic field applied perpendicular to the easy axis makes the ground antiferromagnetic configuration unstable against the phase transformation to the canted phase. On the contrary, if the magnetic field is applied parallel to the easy axis the antiferromagnetic (AF) phase is stable up to the thermodynamic critical field H_T. When the field is further increased, a spin-flop (SF) phase develops in the system. Let us assume that in the antiferromagnetic superconductor the lower critical field fulfills the relation $H_{c1} < \frac{1}{2}H_T$ and that the external field H_0 is applied parallel to the easy axis. When $H_{c1} < H_0 < \frac{1}{2}H_T$ the vortices appear entirely in the AF phase. When H_0 is increased beyond $\frac{1}{2}H_T$ the phase transition to the SF phase originates in the core, because near H_{c1} the field intensity in the core is approximately twice H_{c1} [17]. The spatial distribution of the field across the vortex is a function decreasing from the center as seen in Figure 1. Thus, the magnetic field intensity outside the core is less then H_T and, therefore, the rest of the vortex remains in the AF phase. The radius of a spin-flop domain grows as the field is increased. The formation of domains inside the vortices should be accompanied by the modification of the surface energy barrier [12]. This process leads to a state of the superconductor in which flux entrance is temporarily prohibited – flux density is independent of the applied field. In order to kill this state the external field should be increased above certain second critical field for flux penetration. Then, the vortices penetrating the sample will have the spin flop domains created along the cores. The goal of our work is to compare the model calculations based on the method of images [18] with the experimental results obtained for the $DyMo_6S_8$ single crystal.

Theoretical considerations

In order to describe thermodynamic behavior of $DyMo_6S_8$ for constant temperature and constant external magnetic field we introduce the following free energy functional [2]

$$F = \int \mathrm{d}V \left\{ f_S + f_M + \frac{1}{8\pi}(\mathbf{B} - 4\pi\mathbf{M})^2 \right\} \cdot \qquad (1)$$

Here $\mathbf{B}$ is the magnetic induction, $\mathbf{M} = \mathbf{M}_1 + \mathbf{M}_2$ the magnetization of two sublattices antiferromagnet and $\mathbf{H} = \mathbf{B} - 4\pi\mathbf{M}$ the intensity of thermodynamic magnetic field. The energy density of the superconducting subsystem f_S is expressed in a standard way

$$f_S = \frac{\hbar^2}{2m}\left|\left(\nabla - \frac{2\mathrm{i}e}{c\hbar}\mathbf{A}\right)\Psi\right|^2 + a\left|\Psi\right|^2 + \frac{1}{2}b\left|\Psi\right|^4. \qquad (2)$$

The quantity e, m, c denote charge and mass of the electron and light velocity, respectively. According to experiments the antiferromagnetic order is practically unaffected by the appearance of superconductivity, then it is reasonable to neglect the effect of superconductivity on the exchange interaction in F. This means that both order parameters Ψ and $\mathbf{M}$ are coupled *via* the vector potential $\mathbf{A}$:

$$\nabla \times \mathbf{A} = \mathbf{B} = \mathbf{H} + 4\pi\mathbf{M}$$

$$\mathbf{j}_s = \frac{c}{4\pi}\nabla \times \mathbf{H}, \qquad (3)$$

where $\mathbf{j}_s$ denotes a superconducting current. The antiferromagnetic energy density, which mimics the experimental results in $DyMo_6S_8$, is given by the following expression

$$f_M = J\mathbf{M}_1 \cdot \mathbf{M}_2 + K\sum_{i=1}^{2}(M_i^z)^2 - |\gamma|\sum_{i=1}^{2}\sum_{j=x,y,z}\left(\nabla M_i^j\right)^2. \qquad (4)$$

Here J is the exchange constant between two antiferromagnetic sublattices, K denotes single ion anisotropy constant, and $\sqrt{|\gamma|}$ is the magnetic stiffness length. Since in the following we analyze the phenomena with characteristic length-scales much larger then the interatomic Dy-Dy distance it is justified to omit the gradient term in f_M. The components of the total magnetization vector $\mathbf{M} = \mathbf{M}_1 + \mathbf{M}_2$, $|\mathbf{M}_i| = M_0$ $(i = 1, 2)$ have the following form in both sublattices: $M_{ix} = M_0 \sin\theta_i$, $M_{iy} = 0$, $M_{iz} = M_0 \cos\theta_i$, where θ_i (canted spin angle) is the angle between the magnetization in the sublattice and the external magnetic field directed along z-axis. The AF $(\theta_1 = 0, \theta_2 = \pi)$ and SF phases $(\theta_1 = -\theta_2 = \theta)$ are in

thermodynamic equilibrium in an applied field equal to the thermodynamic critical field:

$$H_T = M_0[K(J-K)]^{1/2}. \tag{5}$$

The canted spin angle of the SF phase is then expressed as

$$\cos\theta = \frac{KM_0}{H_T}\,. \tag{6}$$

The equilibrium conditions of the whole system can be obtained *via* minimization the Gibbs free energy functional $G = F - \frac{1}{4\pi}\int(\mathbf{B}\cdot\mathbf{H}_0)\mathrm{d}V$ with respect to Ψ, $\mathbf{A}$ and $\mathbf{M}$. Performing this task in London approximation one can obtain

$$\mathbf{B} + \lambda^2\nabla\times\nabla\times(\mathbf{B}-4\pi\mathbf{M}) = 0, \tag{7}$$

where λ is the London penetration depth. The appropriate equations describing spatial distribution of $\mathbf{M}$ should accompany equation (7). To make the problem simpler we suppose that the magnetization is constant across the SF domain [12,19]. In this way the distribution of the magnetization around a single vortex is the following

$$|\mathbf{M}| = \begin{cases} M & \text{if } \ r \le r_0 \\ \\ 0 & \text{if } \ r > r_0 \end{cases}, \tag{8}$$

where r_0 is the radius of the spin-flop domain. With the help of equation (7) one can write equation (1) for a single vortex as follows

$$F = \frac{1}{8\pi}\int\left\{(\mathbf{b}_{\mathrm{SF}}-4\pi\mathbf{M})^2 + \lambda^2\left[\nabla\times(\mathbf{b}_{\mathrm{SF}}-4\pi\mathbf{M})\right]^2\right\}\mathrm{d}V_{\mathrm{SF}}$$

$$+\frac{1}{8\pi}\int\left[\mathbf{b}_{\mathrm{AF}}^2 + \lambda^2\left(\nabla\times\mathbf{b}_{\mathrm{AF}}\right)^2\right]\mathrm{d}V_{\mathrm{AF}}. \tag{9}$$

Here $\mathbf{b}_{\mathrm{AF}}$ and $\mathbf{b}_{\mathrm{SF}}$ denote magnetic induction in AF and SF phases of a single vortex, respectively. The integrals are performed over the volume of each phase with the exclusion of the volume of the vortex core. Equation (7), for a single vortex, can be solved in the cylindrical coordinates in terms of the modified Bessel functions K_0 and I_0:

$$b_{\mathrm{SF}} = C_1K_0\left(\frac{r}{\lambda}\right) + C_2I_0\left(\frac{r}{\lambda}\right),\ \text{for } \xi < r \le r_0$$

$$b_{\mathrm{AF}} = C_3K_0\left(\frac{r}{\lambda}\right),\ \text{for } r > r_0, \tag{10}$$

(ξ denotes the coherence length) with the following boundary conditions:

$$b_{\mathrm{SF}}\left(\frac{r_0}{\lambda}\right) = H_T + 4\pi M = B_T$$

$$b_{\mathrm{AF}}\left(\frac{r_0}{\lambda}\right) = H_T. \tag{11}$$

These conditions, together with the flux quantization condition, are used to calculate the arbitrary constants in equation (10).

$$\begin{aligned}
C_1 &= \beta\left[B_T\frac{r_0}{\lambda}I_1\left(\frac{r_0}{\lambda}\right) - \alpha I_0\left(\frac{r_0}{\lambda}\right)\right]\\
C_2 &= \beta\left\{B_T\left[\frac{r_0}{\lambda}K_1\left(\frac{r_0}{\lambda}\right) - 1\right] + \alpha K_0\left(\frac{r_0}{\lambda}\right)\right\}\\
C_3 &= \frac{H_T}{K_0\left(\frac{r_0}{\lambda}\right)}\\
\alpha &= H_T\frac{r_0}{\lambda}\frac{K_1\left(\frac{r_0}{\lambda}\right)}{K_0\left(\frac{r_0}{\lambda}\right)} - \frac{\varphi_0}{2\pi\lambda^2}\\
\beta &= \left\{\frac{r_0}{\lambda}K_1\left(\frac{r_0}{\lambda}\right)I_0\left(\frac{r_0}{\lambda}\right) - I_0\left(\frac{r_0}{\lambda}\right)\right.\\
&\quad\left. +\ \frac{r_0}{\lambda}K_0\left(\frac{r_0}{\lambda}\right)I_1\left(\frac{r_0}{\lambda}\right)\right\}^{-1}.
\end{aligned} \tag{12}$$

Finally, the minimum of the free energy of the vortex per unit length

$$\begin{aligned}
\varepsilon_1 &= \frac{\lambda^2}{8\pi}\oint_{\sigma_1}\mathrm{d}\boldsymbol{l}\left\{[\mathbf{b}_{\mathrm{SF}}-4\pi\mathbf{M}]\times\nabla\times\mathbf{b}_{\mathrm{SF}}\right\}\\
&\quad+\frac{\lambda^2}{8\pi}\oint_{\sigma_2}\mathrm{d}\boldsymbol{l}\left\{\mathbf{b}_{\mathrm{AF}}\times\nabla\times\mathbf{b}_{\mathrm{AF}}\right\},
\end{aligned} \tag{13}$$

with respect to r_0 determines:

$$\left(\frac{r_0}{\lambda}\right)^2 = \frac{\varphi_0}{\pi\lambda^2B_T}\,. \tag{14}$$

The line integrals in equation (13) are performed over the cross-sections perpendicular to the axis of an appropriate cylindrical element of the surface of the vortex, σ_1 denotes the surface of the vortex core, σ_2 the surface of the SF domain.

In order to study the conditions under which magnetic flux density in the sample becomes unstable in the applied magnetic field one must take into account the surface energy barrier preventing vortices from entering or exiting the sample. The presence of a surface of the superconductor leads to the distortion of the field and current of any vortex located within a distance of the order of penetration depth from the surface. The requirement that the currents cannot flow across the surface of the superconductor leads to the introduction of an image vortex, at $x = -x_L$, with vorticity opposite to the real one. Both vortices interact as real ones except that the interaction is attractive.

We consider semi-infinite specimen in the half space $x \ge 0$, the vortex and the external magnetic field running parallel to the surface. In the low flux density regime $\xi^2 < \varphi_0/B < \lambda^2$, Clem [18] has shown the existence of a vortex-free region of the width x_{vf} near the surface of the sample and constant vortex density region for $x > x_{vf}$. Within vortex-free area one can introduce locally averaged magnetic field B_M exponentially decreasing from its surface value H_0 to its average interior value B,

$$B_M = B\cosh\left(\frac{x_{vf}-x}{\lambda}\right). \tag{15}$$

The boundary condition $B_M(0) = H_0$ determines the thickness of the vortex-free region

$$x_{vf} = \lambda \cosh^{-1}\left(\frac{H_0}{B}\right). \tag{16}$$

Now we can characterize the distribution of the magnetic induction around a single vortex in the vortex-free region

$$\begin{aligned} B_{\rm SF} &= b_{\rm SF}\Big(\frac{x-x_L}{\lambda}\Big) - b_{\rm AF}\Big(\frac{x+x_L}{\lambda}\Big) \\ &\quad + B_M\Big(\frac{x_{vf}-x}{\lambda}\Big), \\ B_{\rm AF} &= b_{\rm AF}\Big(\frac{x-x_L}{\lambda}\Big) - b_{\rm AF}\Big(\frac{x+x_L}{\lambda}\Big) \\ &\quad + B_M\Big(\frac{x_{vf}-x}{\lambda}\Big). \end{aligned} \tag{17}$$

The Gibbs free energy of the system can now be written in the following way

$$\begin{aligned} G &= \frac{\lambda^2}{8\pi}\oint_{\sigma_1} {\rm d}\boldsymbol{\sigma}\left\{[\mathbf{B}_{\rm SF} - 2\mathbf{H}_0 - 4\pi\mathbf{M}]\times\nabla\times\mathbf{B}_{\rm SF}\right\} \\ &+ \frac{\lambda^2}{8\pi}\oint_{\sigma_2} {\rm d}\boldsymbol{\sigma}\left\{[\mathbf{B}_{\rm AF} - 2\mathbf{H}_0]\times\nabla\times\mathbf{B}_{\rm AF}\right\} \\ &+ \frac{\lambda^2}{8\pi}\oint_{\sigma_3} {\rm d}\boldsymbol{\sigma}\left\{\hat{z}B_M\times\nabla\times\mathbf{B}_{\rm AF}\right\}, \end{aligned} \tag{18}$$

where σ_3 is the surface of the specimen. After some transformations [12,18], one can obtain the Gibbs free energy per unit length $\mathcal{G}$ in the following form:

$$\begin{aligned} \mathcal{G} &= \varepsilon_1 - \frac{\lambda^2}{4}D_1 b_{AF}\left(\frac{2x_L}{\lambda}\right) \\ &\quad - \frac{\lambda^2}{2}\left[D_1 H_0 - D_2 B_M\left(\frac{x_{vf}-x}{\lambda}\right)\right], \end{aligned} \tag{19}$$

where

$$\begin{aligned} D_1 = &- \xi\left.\frac{{\rm d}b_{\rm SF}\left(\frac{x-x_L}{\lambda}\right)}{{\rm d}x}\right|_{x=x'} - r_0\left.\frac{{\rm d}b_{\rm SF}\left(\frac{x-x_L}{\lambda}\right)}{{\rm d}x}\right|_{x=x''} \\ &- r_0\left.\frac{{\rm d}b_{\rm AF}\left(\frac{x-x_L}{\lambda}\right)}{{\rm d}x}\right|_{x=x''} \\ D_2 = &- \xi\left.\frac{{\rm d}b_{\rm SF}\left(\frac{x-x_L}{\lambda}\right)}{{\rm d}x}\right|_{x=x'} - r_0\left.\frac{{\rm d}b_{\rm SF}\left(\frac{x-x_L}{\lambda}\right)}{{\rm d}x}\right|_{x=x''} \\ &- 2\,r_0\left.\frac{{\rm d}b_{\rm AF}\left(\frac{x-x_L}{\lambda}\right)}{{\rm d}x}\right|_{x=x''} \end{aligned}$$

$$x' = x_L + \xi\ ;\ x'' = x_L + r_0$$

$\mathcal{G}$ has its maximum at $x = x_{max}$ somewhere in the vortex-free region $r_0 < x_{max} < x_{vf}$. We can find x_{max} solving the force balance equation. When the external field reaches

$$H_{en2}(B) = B\cosh\left(\frac{x_{en}}{\lambda}\right), \tag{20}$$

where x_{en} is the vortex-free width corresponding to an external field equal to H_{en2}, the energy barrier moves within a distance r_0 of the surface ($r_0 \ll x_{vf}$). Thus, one can get

$$-\frac{\lambda D_1}{2D_2}\left.\frac{{\rm d}b_{AF}\left(\frac{2x_L}{\lambda}\right)}{{\rm d}x_L}\right|_{x_L=r_0} = B\sinh\left(\frac{x_{en}-r_0}{\lambda}\right). \tag{21}$$

The left hand side of the above equation gives $H_{en2}(0)$. This field may be thought as the second critical field for flux penetration calculated in the single vortex approximation [12].

$$2H_{en2}(0) = \frac{H_T}{\sqrt{\frac{\varphi_0}{\pi\lambda^2 B_T}}\ln\left(\frac{\pi\lambda^2 B_T}{\varphi_0}\right)}. \tag{22}$$

Taking into account that $r_0 \ll x_{en}$ we finally obtain

$$H_{en2}(B) = \sqrt{B^2 + H_{en2}^2(0)}. \tag{23}$$

Let us make a short summary of the calculations. When the SF domain develops, the screening current must redistribute its flow around the vortex in order to fulfill the single flux quantum requirement. This one can easy deduce from equations (10–12). The redistribution of the screening current causes the change in the surface energy barrier preventing vortices from entering into the sample. This is expressed in equation (19). Consequently, the averaged flux density in the sample $B = n\varphi_0$ remains constant when the external field is increased. The vortices start to penetrate into the sample again when the second critical field for flux penetration, calculated in equation (23), is reached.

Experimental details

The single crystals of $DyMo_6S_8$ were grown using the slow cooling of a melted charge closed in hermetically sealed molybdenum ampoules. Details of the crystal grow procedure are described elsewhere [14,20]. The crystals were pure, homogeneous and large enough to be used for studying some subtle effects accompanying the magnetization process at milikelvin temperatures. Chemical composition and crystal uniformity were examined using a Hitachi Scanning Electron Microscope equipped with an energy dispersive X-ray analyzer. Single-crystal X-ray diffraction measurements were performed at room temperature on a Simens SMART CCD diffractometer. The electron probe microanalysis of the regular-shaped crystals showed a composition corresponding to the $DyMo_6S_8$

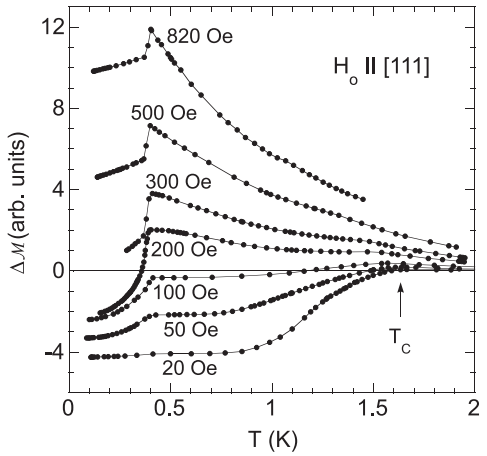

Fig. 2. Magnetization *versus* temperature at several applied fields for $DyMo_6S_8$ single crystal for the field direction oriented parallel to the magnetic easy axis.

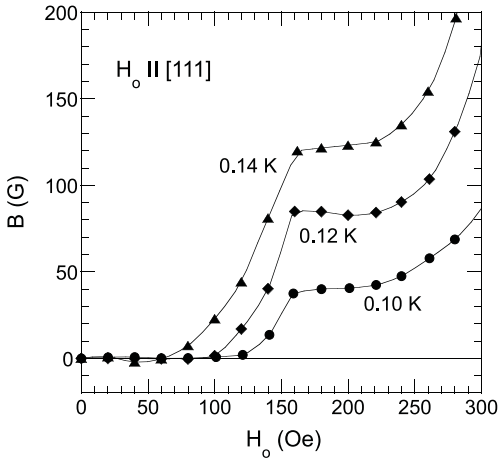

Fig. 3. Magnetic induction for $DyMo_6S_8$ single crystal in the virgin state measured as a function of an applied field for three temperatures below $T_N = 0.4$ K. The field direction is oriented parallel to the magnetic easy axis of the crystal. Each $B(H_0)$ curve exhibits characteristic plateau indicating that a number of vortices is kept constant when the external field is increased. The results are not corrected for demagnetizing effects. The corrected values used for calculations are given in Table 1. The solid lines are guide to the eye.

formula. The cell parameters in the rhombohedral lattice were $a_R = 6.452 \times 10^{-8}$ cm and $\alpha_R = 89.50°$, and were equivalent for all crystals analyzed. The single crystal selected for our experiment had dimensions $0.2 \times 0.2 \times 0.2$ mm^3 and a mass $\simeq 0.05$ mg.

Magnetization was measured with the SHE 330X series SQUID system with SQUID sensor installed in the vacuum chamber of the ^{3}He $-^4$He dilution refrigerator. The sensor was thermally anchored to the liquid He bath (4.2 K) and shielded with a Nb tube. Two counter-wound pickup coils were connected to the input coil of the SQUID sensor. The SQUID pickup coils were placed in the center of a 10 cm long superconducting solenoid generating a magnetic field up to 1.5 kOe. Both the coils and the solenoid were fixed to the mixing chamber of the dilution refrigerator. Details of the experimental setup are described elsewhere [14]. The perfect shielding ($4\pi\mathcal{M} = H_0$) of the Meissner state was used to calibrate the SQUID system. The crystal was oriented with the magnetic easy axis (the [111] crystallographic triple axis) parallel to the external magnetic field. For this orientation, the demagnetizing factor was assumed to be $k = 1/3$.

Comparison with theory

In Figure 2, the magnetization $\mathcal{M}$ measured as a function of temperature is presented for several applied magnetic fields oriented parallel to the easy axis of the single crystal. At higher temperatures, the transition to the superconducting state is observed at T_c as the smooth decrease of $\mathcal{M}$ (*e.g.*, $T_c = 1.62$ K for $H_0 = 20$ Oe). This critical temperature is clearly field dependent as expected for a superconductor. At low fields, $\mathcal{M}$ riches negative values close to T_c. At higher fields, this is not possible because of the induced strong paramagnetic moment of the Dy ions. At low temperatures, the abrupt change of $\mathcal{M}$ is observed at $T_N = 0.4$ K, reflecting the transition to the AF state. In that state, the internal field is reduced and $\mathcal{M}$ can now become negative even for higher fields. At T_N and for $H_0 \leq 200$ Oe, the change of $\mathcal{M}$ between the paramagnetic (PM) and AF states increases significantly with increasing field, as expected. However, for $H_0 > 200$ Oe, the single crystal is in the SF phase [15,16] and the observed change of $\mathcal{M}$, caused by the transition to the ordered state, now decreases with increasing field.

The low-field parts of the $B(H_0)$ virgin curves are presented in Figure 3 to show the details of flux penetration. These curves have been obtained by the simple transformation of the $\mathcal{M}(H_0)$ results reported in our previous work [14]. The observed penetration is typical above $T_N = 0.4$ K and proceeds as an unusual two-stage process at lower temperatures where AF order coexists with superconductivity. At low fields the sample is in the Meissner state. When the field increases above H_{c1}, the sample is penetrated by the flux. Then, at higher fields, the penetration process stops unexpectedly and $B = B_{pl}$ is constant in the sample while the external field is further increased. This new perfect shielding appears at $H = H_{pl}$. The penetration process starts again when the field reaches $H = H_{en2}$. This value we call the second critical field for flux penetration.

An interesting effect of the temperature dependence of H_{c1} below T_N is seen in Figure 3 and Table 1. The very small decrease in temperature results in the significant increase of H_{c1}, whereas H_{c2} measured by us in 0.1 K, 0.12 K, and 0.14 K remains close to 900 Oe. The similar behavior has been observed in $GdMo_6Se_8$, its main feature is a sharp dip on the $H_{c1}(T)$ around T_N and a plateau on $H_{c2}(T)$ for $T < T_N$ [21]. This behavior agrees well with our theoretical model. The large increase of H_{c1} for

Table 1. Experimental values of Figure 3 corrected for demagnetizing effects according to the formulae: $H = H_0 + 4\pi k\mathcal{M}$, and $B = H - 4\pi(1-k)\mathcal{M}$ [24], where $\mathcal{M}$ (absolute value) is taken from Figure 4 of reference [14].

T [K]	κ	H_{c1} [Oe]	H_{pl} [Oe]	B_{pl} [G]	$H_{en2}(B)$ [Oe]
0.14	4.3	100	170	135	250
0.12	3.1	150	185	105	270
0.10	2.6	180	200	80	280

temperatures decreasing below T_N indicates that our sample is in the antiferromagnetic collinear phase. In this phase, when temperature decreases from T_N, the pair-breaking effects due to molecular field and antiferromagnetic fluctuations weaken and $H_{c1}(T)$ rapidly tends to match its pattern in the paramagnetic state. On the contrary, the nearly constant H_{c2} below T_N [22,23] indicates that the sample is in the antiferromagnetic canted phase and pair-breaking effects due to the on-field component of the molecular field are present even at the lowest temperatures. In our model we have assumed that vortices enter the sample in the collinear antiferromagnetic state, and when the field is increased the canted phase appears first inside the core of the vortex. Thus, above H_{en2}, if the external field is further increased the volume of the canted phase enlarges. This makes possible to transform the whole sample to the canted phase well below H_{c2}.

In order to compare our theoretical model with the experimental results we have estimated several quantities. The most important is the Ginzburg-Landau (GL) parameter κ. This parameter has been calculated in [14] to be equal to 2.6 for $T = 0.10$ K. We have taken advantage of the strange behavior of $H_{c1}(T)$ and $H_{c2}(T)$ to calculate κ for $T = 0.14$ K and $T = 0.12$ K. The constant value of $H_{c2} = 900$ Oe in the range of $0.10\ \text{K} \leq T \leq 0.14$ K predicts that coherence length does not change in this interval of temperatures where an abrupt increase of H_{c1} suggests that the penetration depth drastically decreases. This observation has been used to write the following equation

$$\frac{H_{c1}(T_0)}{H_{c1}(T)} = \left(\frac{\kappa(T)}{\kappa(T_0)}\right)^2 \frac{\ln\kappa(T_0)}{\ln\kappa(T)}, \tag{24}$$

where $T_0 = 0.10$ K , $\kappa(T_0) = 2.6$ and $0.12\ \text{K} \leq T \leq 0.14$ K. The above equation has been solved numerically and the results for κ are given in Table 1.

To find the thermodynamic critical field H_T and then to calculate $H_{en2}(B)$ we have used the following argumentation. At low fields, in the vicinity of the lower critical field H_{c1}, the intensity of the field in the vortex core is $2H_{c1}$ [17]. When the external field is increased the field intensity in the vortex core increases because of the superposition of the fields of the surrounding vortices. The field intensity in the core must reach H_T in order to originate the transition to the SF phase. Thus, taking into account only the nearest z neighbors we can write

$$H_T = 2H_{c1} + z\frac{\varphi_0}{2\pi\lambda^2}K_0\left(\frac{d}{\lambda}\right), \tag{25}$$

Table 2. Summary of the calculated quantities.

T [K]	d/λ	H_T [Oe]	$4\pi M$ [G]	B_T [G]	$H_{en2}(B)$ [Oe]
0.14	1.7	250	1000	1250	215
0.12	2.8	325	775	1100	240
0.10	4.9	360	700	1060	265

where d denotes intervortex spacing, and d/λ corresponds to the value B_{pl} for which the penetration process unexpectedly stops. The relations $B_\Delta = 2\varphi_o/d^2\sqrt{3}$ (for triangular lattice of vortices), $\varphi_o = 2\pi H_{c2}\xi^2$, where $H_{c2} = 900$ Oe [14] have been used to obtain d/λ. Then, this value has been inserted into equation (25) to obtain H_T. The saturation magnetization of Dy ions, $8\pi M_0 = 3780$ G has been calculated taking into account the volume of the elementary cell of $DyMo_6S_8$, $V = 268 \times 10^{-24}$ cm^3. The anisotropy coefficient $K = 0.44$ has been determined for each magnetization curve by finding the best fit of the theoretical with the experimental magnetization curves [25]. Next, the magnetization in the SF-phase domain has been calculated with the help of equation (6)

$$M = 2M_0\cos\theta = \frac{2KM_0^2}{H_T}\,. \tag{26}$$

Equation (26) gives M corresponding to the field H_{pl} for which the penetration stops. Finally, inserting all the above calculated values into equations (22, 23) we have obtained $H_{en2}(B)$. The results are summarized in Table 2.

Conclusion

We have demonstrated that the antiferromagnetic superconductor $DyMo_6S_8$ shows interesting behavior in the magnetic field applied below T_N. The sample in the virgin state magnetizes initially like ordinary type II superconductor. When the applied magnetic field reaches the critical field for flux penetration the sample transforms from the Meissner to the mixed state. Then, magnetization proceeds in an unusual way. As the field is further increased, a new shielding state appears but, in the contrary to the Meissner state, with a constant flux density inside the sample. Characteristic plateau, observed for the magnetization curves, proofs that magnetic flux density inside $DyMo_6S_8$ is unaffected by the increased external field. When the field reaches certain value, we call it the second critical field for flux penetration, the flux starts to enter the sample again. This phenomenon we name two-step flux penetration. We have argued that in this new state vortices transform to the shape shown in Figure 1, where a domain of the spin-flop phase is created. The expected metamorphosis of the vortices leads to a spatial redistribution of the shielding supercurrents, flowing around the core, in order to keep constant the flux carried by each vortex. Consequently, a new energy barrier is formed near the surface preventing vortices from entering the sample. Thus, the number of vortices inside the superconductor is kept constant. To overcome the new energy barrier by the

vortices with magnetic structure the external field must be increased beyond H_{en2}, the second critical field for flux penetration. The formula for this field has been derived using the image method. The values of H_{en2} calculated for three temperatures below T_N agree very well with the experimental results.

We would like to thank Prof. J. Sznajd, Prof. T. Kopeć, and Dr. P. Tekiel for helpful discussions. This work was supported by the State Committee for Scientific Research (KBN) within the Project No. 2 P03B 125 19.

References

1. For review see *Superconductivity in Ternary Compounds*, edited by M.B. Maple, Ø. Fischer (Springer-Verlag, Berlin, 1982)
2. L.N. Bulaevskii, A.I. Buzdin, M. Kulić, S.V. Panjukov, Adv. Phys. **34**, 176 (1985), Sov. Phys. Uspekhi **27**, 927 (1984)
3. M.B. Maple, Physica B **215**, 110 (1995)
4. L. Bauernfeind, W. Widder, H.F. Braun, Physica C **254**, 151 (1995)
5. D.J. Pringle, J.L. Tallon, B.G. Walker, H.J. Trodahl, Phys. Rev. B **59**, R11679 (1999)
6. P.W. Klamut, B. Dabrowski, S. Kolesnik, M. Maxwell, J. Mais, Phys. Rev. B **63**, 224512 (2001)
7. M. Houzet, A.I. Buzdin, M. Kulić, Phys. Rev. B **64**, 184501 (2001)
8. S.S. Saxena, P. Agarwal, K. Ahilan, F.M. Grosche, R.K.W. Haselwimmer, M.J. Steiner, E. Pugh, I.R. Walker, S.R. Julian, P. Monthoux, G.G. Lonzarich, A. Huxley, I. Sheikin, D. Braithwaite, J. Flouquet, Nature **406**, 587 (2000)
9. C. Pfleiderer, M. Uhlarz, S.M. Hayden, R. Vollmer, H.V. Lohneysen, N.R. Bernhoeft, G.G. Lonzarich, Nature **412**, 58 (2001)
10. N.K. Sato, N. Aso, K. Miyake, R. Shiina, P. Thalmeier, G. Varelogiannis, C. Geibel, F. Steglich, P. Fulde, T. Komatsubara, Nature **410**, 340 (2001)
11. T. Krzysztoń, J. Magn. Magn. Mater. **15-18**, 1572 (1980)
12. T. Krzysztoń, Phys. Lett. A **104**, 225 (1984)
13. H. Iwasaki, M. Ikebe, Y. Muto, Phys. Rev. B **33**, 4669 (1986)
14. K. Rogacki, E. Tjukanoff, S. Jaakkola, Phys. Rev. B **64**, 094520 (2001)
15. W. Thomlinson, G. Shirane, D.E. Moncton, M. Ishikawa, Ø. Fischer, J. Appl. Phys. **50**, 1981 (1979)
16. W. Thomlinson, G. Shirane, J.W. Lynn, D.E. Moncton, in *Superconductivity in Ternary Compounds*, edited by M.B. Maple, Ø. Fischer (Springer-Verlag, Berlin 1982)
17. M. Tinkham, *Introduction to Superconductivity*, Chap. 5 (McGraw-Hill Inc., New York 1975)
18. J.R. Clem, in *Proceedings of the 13th Conference on Low Temperature Physics (LT 13)*, Vol. 3 (Plenum-Press, New York 1974), p. 102
19. A.I. Buzdin, S.S. Krotov, D.A. Kuptsov, Solid State Commun. **75**, 229 (1990)
20. R. Horyń, O. Pena, C. Geantet, M. Sergent, Supercond. Sci. Technol. **2**, 71 (1989)
21. K. Rogacki, Cz. Sułkowski, Physica C **153-155**, 483 (1988)
22. M. Ishikawa, Contemp. Phys. **23**, 443-468 (1982)
23. M. Ishikawa, J. Muller, Solid State Commm. **27**, 761 (1978)
24. L.D. Landau, E.M. Lifshitz, *Electrodynamics of continuous media*, Chap. 6 (Oxford, Pergamon Press 1960)
25. A.H. Morrish, *The Physical Principles of Magnetism*, Chap. 6 (John Wiley and Sons, Inc. New York 1965)